Applied Catalysis B: Environmental 331 (2023) 122682

Contents lists available at ScienceDirect

Applied Catalysis B: Environmental

journal homepage: www.elsevier.com/locate/apcatb

High-temperature water oxidation activity of a perovskite-based nanocomposite towards application as air electrode in reversible protonic ceramic cells

Mingzhuang Liang [a,1], Yuhao Wang [b,c,1], Yufei Song [b,c,1], Daqin Guan [e], Jie Wu [a], Peng Chen [a], Adeleke Maradesa [b,c], Meigui Xu [a,*], Guangming Yang [a], Wei Zhou [a], Wei Wang [a], Ran Ran [a], Francesco Ciucci [b,c,d,**], Zongping Shao [f,*]

[a] State Key Laboratory of Materials-Oriented Chemical Engineering, College of Chemical Engineering, Nanjing Tech University, Nanjing 210009, PR China
[b] Department of Mechanical and Aerospace Engineering, The Hong Kong University of Science and Technology, Clear Water Bay, Hong Kong, China
[c] HKUST Shenzhen-Hong Kong Collaborative Innovation Research Institute, Futian, Shenzhen 518048, PR China
[d] Energy Institute, The Hong Kong University of Science and Technology, Clear Water Bay, Hong Kong, China
[e] Department of Building and Real Estate, Research Institute for Sustainable Urban Development (RISUD) and Research Institute for Smart Energy (RISE), The Hong Kong Polytechnic University, Hung Hom, Kowloon, Hong Kong, China
[f] WA School of Mines: Minerals, Energy and Chemical Engineering (WASM-MECE), Curtin University, Perth, WA 6845, Australia

ARTICLE INFO

Keywords:
Reversible protonic ceramic cells
Nanocomposite
Perovskite
Air electrode
Water electrolysis

ABSTRACT

Reversible protonic ceramic cells (r-PCCs) can operate alternately in fuel cell and electrolysis cell modes, while their practical applications are limited due to the lack of air electrodes with high oxygen reduction/evolution reaction (ORR/OER) activities. A nanocomposite $Ba_{0.95}(Co_{0.4}Fe_{0.4}Zr_{0.1}Y_{0.1})_{0.95}Ni_{0.05}O_{3-\delta}$ (BCFZYN), consisting of a major perovskite phase (D-BCFZYN) and a minor NiO phase, has demonstrated outstanding ORR activity in protonic ceramic fuel cells [1]. Herein, we experimentally and theoretically demonstrate that BCFZYN possesses excellent OER activity. Density functional theory calculations indicate that NiO nanoparticles enhance water adsorption while D-BCFZYN accelerates oxygen desorption and proton conduction, thus promoting OER kinetics. A cell with BCFZYN air electrode achieved a current density of − 1267 mA cm^{-2} at 1.3 V at 600 °C, while maintaining favorable durability of 372 h. The corresponding cell demonstrated stable operation during cycling mode between fuel cell and electrolysis modes, suggesting the material has great potential as an air electrode for r-PCCs.

1. Introduction

Global excessive use of fossil fuels, such as oil and natural gas, has caused severe environmental pollution and greenhouse gas effects. Renewable energy sources, such as solar and wind energy, are expected to contribute significantly to a sustainable global power supply while contributing to a cleaner environment in the future. However, solar or wind energy is diurnally or seasonally intermittent, requiring the integration of highly efficient energy conversion and storage devices for practical use. Unfortunately, conventional batteries are unsuitable for long-term seasonal storage due to self-discharge and high-cost challenges. On the other hand, solid oxide electrolysis cells (SOECs) can efficiently convert renewable electricity to chemical fuels, significantly alleviating the self-discharge and high-cost challenges associated with batteries [2–4]. The re-conversion of H_2 to electric power can be realized through fuel cell technology. Therefore, the development of reversible ceramic cells (r-CCs) allows their perfect integration into renewable energy sources, providing a promising sustainable energy system for the future [5,6].

According to different electrolyte types, r-CCs can be divided into

* Corresponding authors.
** Corresponding author at: Department of Mechanical and Aerospace Engineering, The Hong Kong University of Science and Technology, Clear Water Bay, Hong Kong, China
E-mail addresses: xumeigui@njtech.edu.cn (M. Xu), francesco.ciucci@ust.hk (F. Ciucci), shaozp@njtech.edu.cn (Z. Shao).
[1] These authors contributed equally to this work.

https://doi.org/10.1016/j.apcatb.2023.122682
Received 22 November 2022; Received in revised form 27 February 2023; Accepted 22 March 2023
Available online 23 March 2023

oxygen-ion electrolyte-based (r-OCCs) and proton electrolyte-based cells (r-PCCs) [7]. Compared to r-OCCs, r-PCCs have several unique advantages. First, since the activation energy of proton conduction is lower than that of oxygen-ion conduction in oxides, r-PCCs can operate at a lower temperature range, resulting in improved thermal cycling tolerance and reduced system costs. Second, during electrolysis mode, pure H_2 produced at the fuel electrode can be compressed and stored with no need for a complex drying process, thereby reducing system complexity and cost. Third, water is generated at fuel cell mode and introduced at the air electrode during electrolysis modes, thereby effectively inhibiting the oxidation of Ni catalysts at the fuel electrode [8,9].

Despite great promise, the lack of proper air electrode materials with exceptional activities for oxygen reduction/evolution reactions (ORR/OER) and durability is the biggest obstacle to commercializing r-PCC technology [10,11]. In particular, to achieve high OER activity, the air electrode needs to meet the requirements of high steam/oxygen diffusion, surface exchange, and H^+/e^- mixed conductivity [12,13]. In addition, in r-PCCs, air electrode materials also need to possess stable chemical properties under high-temperature dry/humidified air atmospheres and matchable thermal compatibility with electrolytes to ensure long-term operation [14,15]. However, many reported electrode materials can only meet one or more of these requirements, whereas few can meet all the requirements simultaneously. For example, conventional mixed oxygen ion and electron conducting perovskite air electrodes, such as $La_{0.8}Sr_{0.2}CoO_{3-\delta}$, $La_{0.6}Sr_{0.4}Co_{0.2}Fe_{0.8}O_{3-\delta}$ and $Ba_{0.5}Sr_{0.5}Co_{0.8}Fe_{0.2}O_{3-\delta}$, [16–18] show a lack of proton conductivity and poor chemical stability under humidified air, resulting in poor activity and operational stability. Although $BaCe_{0.5}Bi_{0.5}O_{3-\delta}$, $BaZr_{0.6}Co_{0.4}O_{3-\delta}$, $BaZr_{0.5}Pr_{0.3}Y_{0.2}O_{3-\delta}$, and cobalt-substituted $BaZr_{0.1}Ce_{0.7}Y_{0.2}O_{3-\delta}$ show a certain level of proton conductivity [19–22], the low oxygen-ion and electronic conductivity significantly limit their electrochemical activity. $LnBaCo_2O_{5+\delta}$ (Ln═Gd, Nd, Pr)-based double perovskite materials, such as $NdBa_{0.5}Sr_{0.5}Co_{1.5}Fe_{0.5}O_{5+\delta}$ and $PrBa_{0.5}Sr_{0.5}Co_{1.5}Fe_{0.5}O_{5+\delta}$, have been characterized as materials with high proton concentration, achieving a satisfactory performance in r-PCC technology at the initial stage, [23,24] while Sr segregation under humidified operation conditions, especially high-steam content during electrolysis operation, resulted in severe performance degradation.

With more in-depth investigation, it was found that developing single-phase perovskite air electrode materials to achieve high activity and durable performance for both OER and ORR is incredibly challenging. More recently, composite air electrode materials have attracted extensive attention as an electrode in r-PCCs. Compared to single-phase materials, composite materials are better at meeting the need for various requirements due to the unique functionalities of each phase in the composite [25]. Traditional physical mixing and infiltration methods have been used to develop composite air electrode materials. For example, Wang et al. physically mixed $Ba_{0.5}Sr_{0.5}Co_{0.7}Fe_{0.2}Ni_{0.1}O_{3-\delta}$ mixed O^{2-}/e^- conductor and $BaZr_{0.1}Ce_{0.7}Y_{0.1}Yb_{0.1}O_{3-\delta}$ proton conductor to develop a triple-conducting air electrode, which achieved sufficient electrochemical activity in protonic ceramic electrolysis cell (PCEC) mode [26]. Liu et al. infiltrated $BaCoO_{3-\delta}$ (BCO) into conventional LSCF to develop a BCO-coated LSCF composite air electrode, in which BCO facilitated the oxygen surface exchange process, thereby improving OER activity [27]. Similarly, $La_{1.2}Sr_{0.8}NiO_{4-\delta}$-infiltrated $BaCe_{0.68}Zr_{0.1}Y_{0.1}Yb_{0.1}Cu_{0.02}O_{3-\delta}$, $Ba_{0.5}Gd_{0.8}La_{0.7}Co_2O_{6-\delta}$-infiltrated $BaZr_{0.8}Y_{0.2}O_{3-\delta}$, and $LaCoO_{3-\delta}$-infiltrated $BaZr_{0.8}Y_{0.2}O_{3-\delta}$ also showed favorable activity for OER in PCEC mode [28–30]. Unfortunately, the above materials developed via physical mixing and infiltration methods usually showed limited reaction regions due to the large grain size of each phase and weak connection between multi-phases, thus leading to insufficient activity and poor operational stability [31,32].

Very recently, we developed a nanocomposite, consisting of a major A-site deficient perovskite phase $Ba_{0.99}(Co_{0.4}Fe_{0.4}Zr_{0.1}Y_{0.1})_{0.99}Ni_{0.01}O_{3-\delta}$ (D-BCFZYN) and a minor surface-enriched NiO phase, via selective cation exsolution strategy. The new nanocomposite displayed bifunctionality, sufficient active sites, and a strong connection between multiple phases, realizing both superior ORR activity and robust durability [1]. However, the performance study of BCFZYN in the electrolysis operation is missing. In addition, the fundamental insights underpinning the oxygen exchange kinetics and the role of multiple phases in BCFZYN on electrochemical activity and stability are still poorly understood.

Herein, the BCZFYN nanocomposite air electrode is investigated for its performance (activity and durability) in PCECs, with practical and theoretical evaluation via density functional theory (DFT) calculations. It is found the PCEC with BCFZYN composite as air electrode achieves a current density of − 1267 mA cm^{-2} in electrolysis mode at 1.3 V at 600 °C, and has robust electrolysis durability of 372 h at 550 °C. DFT calculation results suggest the excellent OER activity could be attributed to the rapid steam adsorption on the NiO nanoparticles, and fast O_2 desorption and proton conduction of D-BCFZYN major phase. In addition, the cell also operates stably for 194 h during cycling mode between fuel cell and electrolysis modes, showing great commercial potential in r-PCCs.

2. Experiment

2.1. Materials synthesis

The $BaZr_{0.1}Ce_{0.7}Y_{0.1}Yb_{0.1}O_3$ (BZCYYb), $BaCo_{0.4}Fe_{0.4}Zr_{0.1}Y_{0.1}O_{3-\delta}$ (BCFZY), and BCFZYN perovskite powders were synthesized by an ethylenediaminetetraacetic acid (EDTA) - citric acid monohydrate (CA) complexing method. Taking BZCYYb as an example, $Ba(NO_3)_2$, $Ce(NO_3)_4{\cdot}6\ H_2O$, $Zr(NO_3)_4{\cdot}5\ H_2O$, $Y(NO_3)_3{\cdot}6\ H_2O$, $Yb(NO_3)_3{\cdot}5\ H_2O$ were dissolved in heated water by specific stoichiometric amounts, and then EDTA, CA, and ammonia were added in the solution. The molar ratio of metal ion, EDTA, and CA was 1:1:2. The gel was formed with water evaporated from the solution and then dried to obtain the black precursor. Finally, the precursor was calcined at 1000 °C for 5 h to obtain the BZCYYb powder.

2.2. Cell fabrication

To access the electrochemical activity of the electrode, symmetrical cells were fabricated. 0.4 g BZCYYb powder was dry-pressed into a substrate and then sintered at 1450 °C for 5 h to densify the substrate. The BCFZYN electrode was attached to the electrolyte by spraying method. To obtain the BCFZYN electrode slurry, 1 g BCFZYN power, 10 mL isopropanol, 2 mL ethylene glycol, and 0.8 mL glycerol were placed into a ball mill tank and ground for 30 min. Then, the electrode slurry was sprayed onto the two sides of BZCYYb substrate and calcined at 900 °C for 2 h. Finally, the silver paste was brushed onto the electrode to collect the current and silver wires were connected to the electrode to obtain an integral symmetrical cell. To investigate electrochemical performance of the electrode in practice, several single cells were also prepared by dry-pressed method. 0.35 g anode powder (NiO:BZCYYb: PVB = 6:4:1) was first dry-pressed into an anode substrate and 0.015 g BZCYYb powder was spread on the anode. Then, the substrate was sintered at 1450 °C for 10 h to densify the BZCYYb electrolyte. Next, the electrode slurry was sprayed onto the side of BZCYYb electrolyte and calcined at 900 °C for 2 h. Finally, the silver paste was brushed onto the electrode side and silver wires were connected to the electrode to obtain a complete single cell.

2.3. Electrochemical measurements

To measure the impedances of symmetrical cells and r-PCCs, the combined test system of a potentiostat (Solartron 1287) and a frequency response analyzer (Solartron 1260) was employed. Symmetrical cells were examined under the conditions of air, 5 vol% H_2O-air, 30 vol% H_2O-air, and 30 vol% H_2O-N_2. A Keithley 2420 source meter was employed to measure I-V curves of r-PCCs and electrical conductivity

relaxation (ECR) curves of the electrodes by the four-probe method. Taking the example of BCFZYN, 0.6 g powders were dry-pressed into a bar and then calcined at 1200 °C for 10 h. Four silver wires were attached to both ends of the bar. The ECR test was carried out with a sudden switch in the oxygen partial pressure from 0.21 to 0.1 atm with 0 vol%, 5 vol%, and 30 vol% H_2O.

2.4. Characterizations

The phase structures of the samples were examined by powder X-ray diffraction (XRD, Philips Advance Bruker) with filtered Cu-Kα radiation (40 kV and 40 mA). The microstructure of BCFZYN was investigated by field emission scanning electron microscopy (FE-SEM, JEOL JSM-7100 F). To investigate the existence and size of NiO nanoparticles in the BCFZYN sample, energy-dispersive X-ray (EDX) mapping was conducted. Rietveld refinement of XRD patterns was used to further analyze the composition and content of each component.

2.5. Computational methods

The supercell program was used to generate atomic 3 × 3 × 3 supercell arrangements of BCFZY-Co and pristine-BCFZYN [33]. The supercell program outputted the five lowest electrostatic ground-state energy configurations after traversing all possible randomly generated structures separately (2.1×10^{12} configurations for BCFZY-Co and 2.3×10^{12} configurations for pristine-BCFZYN). These five configurations were then used to determine the lowest energy ground-state by density functional theory (DFT). D-BCFZYN was the lowest ground state energy configuration obtained by comparing the various A-site defective pristine-BCFZYN configurations (Fig. S1, Supporting Information).

The Vienna ab initio simulation package (VASP) package was utilized for all DFT calculations [34]. The projector augmented wave pseudopotentials, spin-polarization, and the Perdew, Burke, and Ernzerhof functional level of theory under the generalized gradient approximation scheme for electron exchange correlation were used [35]. The strongly correlated Co-3d, Fe-3d, and Ni-3d electrons were modeled using the DFT+U approach with the U_{eff} value set at 3.32 eV, 5.3 eV, and 6.2 eV, consistent with the Materials Project [36]. The energy cutoff for the plane-wave basis set was 450 eV. The Brillouin zone was sampled using a 4 × 4 × 4 Monkhorst-Pack *k*-point mesh. The Broyden method was employed for structural relaxation with the convergence of 0.02 eV/Å and 10^{-5} eV on the force and energy, respectively.

The oxygen vacancy formation energy E_{Vo}^{F} was calculated as

$$E_{Vo}^{F} = E_{defect} - E_{host} + \frac{1}{2}(E_{O_2} + \Delta h) \quad (1)$$

where E_{defect} denotes the energy of the perovskite with an oxygen vacancy, E_{O_2} is the energy of O_2 and $\Delta h = 1.4$eV is the overbinding correction [37].

The hydration energy, ΔE_{hydr}, was calculated as

$$\Delta E_{hydr} = E_{2OH_O^{\bullet}} - E_{defect} + E_{H_2O}(g) \quad (2)$$

where $E_{2OH_O^{\bullet}}$ is the electronic energy of the perovskite with two protons (i.e., two -OH groups), and $E_{H_2O}(g)$ is the energy of a water molecule [38].

The (011)-surface of D-BCFZYN and (111)-surface of NiO were cleaved to calculate OER/ORR and H_2O/O_2 adsorption energies. This is consistent with the TEM image. The vacuum layer of 15 Å along the *c* direction was added to minimize the interactions between the top and bottom layers of the slab. The Brillouin zone was sampled by a 4 × 4 × 1 Monkhorst-Pack k-point mesh.

The free energy diagrams of OER/ORR developed by Rossmeisl and Nørskov et al. were employed to calculate the OER/ORR overpotential (η) [39]. The Gibbs free energy ΔG change from initial to final reaction states were calculated as follows:

$$\Delta G = \Delta E + \Delta ZPE - T\Delta S \quad (3)$$

where T is temperature, ΔS is the entropy change, ΔE is the electronic energy change obtained from the ground-state DFT calculations, ΔZPE is the zero-point energy change of adsorbates [40].

3. Results and discussion

3.1. Phase structure and OER activity analysis

Following our previous study, the NiO nanoparticles modified perovskite BCFZYN nanocomposite was synthesized by the in-situ exsolution strategy. [1,41] The XRD pattern displayed in Fig. S2 (Supporting Information) confirms the synthesized sample is a mixture of a cubic perovskite major phase and a minor phase NiO, as expected. With the combination of SEM, STEM, and EDX characterization results (Fig. S3 and S4, Supporting Information), it can be confirmed that the material is in a nanocomposite structure with NiO nanoparticles modified on the surface of D-BCFZYN, suggesting the good repeatability of the synthesis technique.

OER activity of a PCEC air electrode is related to steam/oxygen diffusion, surface exchange, and H^+/e^- mixed conductivity [42]. Here, electrochemical impedance spectroscopy (EIS) and distribution of relaxation time (DRT) were first used to analyze the oxygen/-proton/electron properties of air electrode materials [43,44]. We first conducted symmetric cell measurement under humidified N_2 to eliminate the effects of O_2. A comparative study of BCFZYN nanocomposite and the simple perovskite BCFZY was conducted. As seen in Fig. 1a, under 30 vol% H_2O-N_2 atmospheres, the polarization resistance (Rp) values and the corresponding activation energy of the BCFZYN electrode are much lower than those of the BCFZY electrode, indicating superior activity of the BCFZYN electrode for OER. DRT analysis can provide useful information about the electrochemical processes. DRTtools was used to compute the DRT calculation [45]. As seen in Fig. 1b, each DRT profile falls into three regions, in which the high-frequency region (P1) represents the transfer process of ions from electrolyte to air electrode at triple-phase boundary, and the intermediate frequency region (P2) represents surface exchange and ionic bulk diffusion processes, while the low-frequency region (P3) represents gas diffusion process [46,47]. As seen in Fig. 1b, the integral area of P3 in BCFZYN air electrode is bigger than that of BCFZY, suggesting the lower steam diffusion capability of BCFZYN. Meanwhile, compared to BCFZY, the integral area of P2 in BCFZYN significantly decreased under 30 vol% H_2O-N_2 atmosphere at 550 °C, suggesting the BCFZYN electrode possesses a faster steam surface exchange capability and higher proton conductivity, which contribute to its higher OER activity.

Considering that PCEC usually operates at high steam content and oxidizing atmospheres, we also conducted symmetric cells measurement under 30 vol% H_2O-air atmosphere (Fig. 1c). The Rp values and the corresponding activation energy of the BCFZYN electrode are lower than that of the BCFZY electrode, suggesting a higher electrochemical activity in the BCFZYN electrode. According to DRT analysis (Fig. 1d), compared to BCFZY, the decreased P3 of the BCFZYN electrode suggests a higher O_2 diffusion capability, which is also beneficial to OER activity.

To further evaluate the surface exchange properties of the electrode material (k_{chem}) associated with OER activity, we conducted electronic conductivity relaxation (ECR) measurements under dry and humidified oxidizing atmospheres. The k_{chem} values were acquired through fitting ECR data of the BCFZY and BCFZYN electrode materials (Fig. S5,6, Supporting Information). It should be noted that under humidified oxidizing atmospheres (5, 30 vol% H_2O), the k_{chem} values of both materials decreased compared to that in dry oxidizing atmospheres, which can be explained by the fact that hydration decreases the oxygen vacancy concentration, thus inhibiting oxygen surface exchange (Fig. S7,

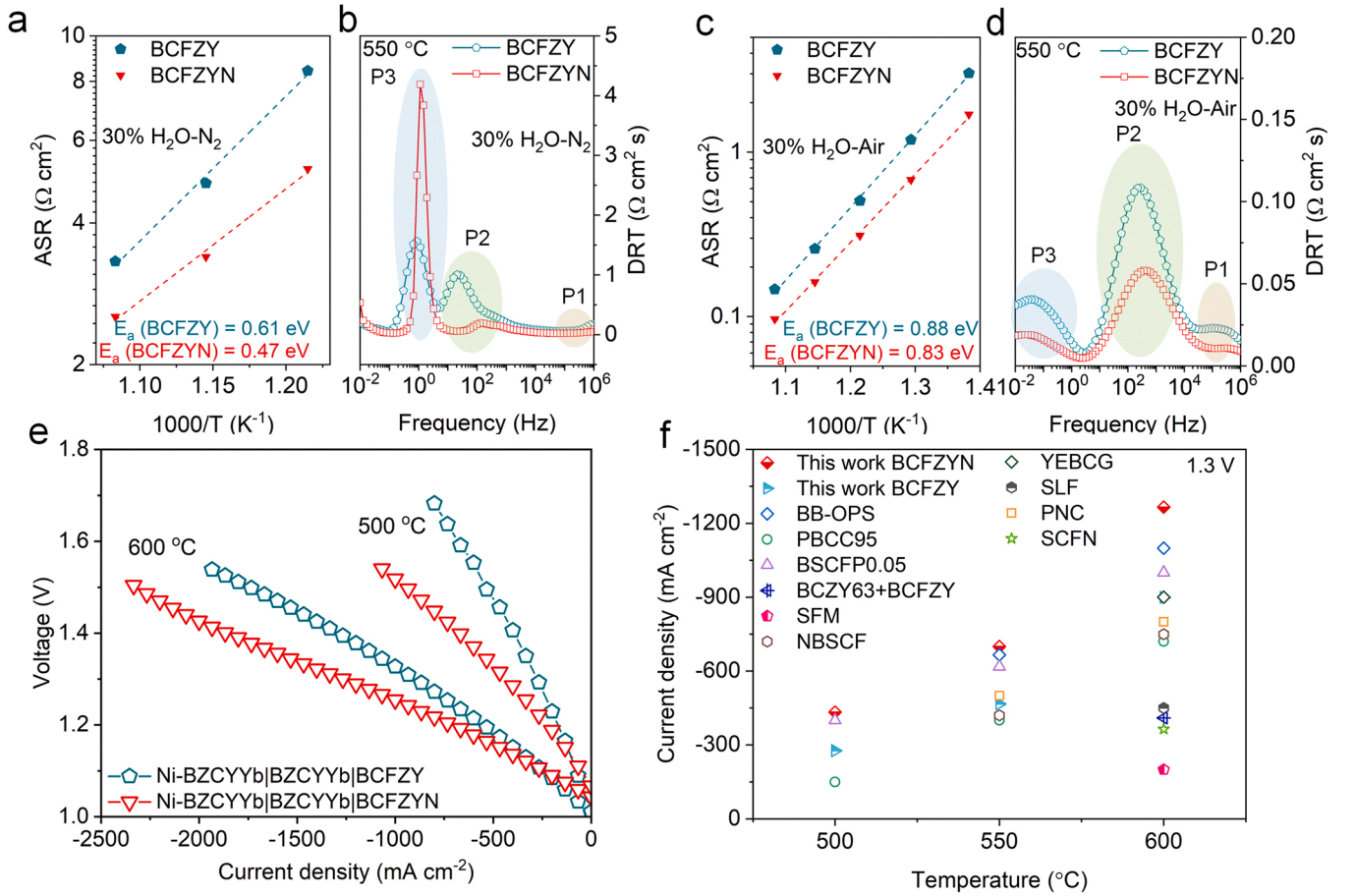

Fig. 1. a) Arrhenius plots of the Rp values of the symmetric cells based on BZCYYb with BCFZY and BCFZYN as electrodes under 30 vol% H_2O-N_2 and b) DRT of BCFZYN and BCFZY electrodes at 550 °C. c) Arrhenius plots of the Rp values of the symmetric cells based on BZCYYb with BCFZY and BCFZYN as electrodes under 30 vol% H_2O-Air and d) DRT of BCFZYN and BCFZY electrodes at 550 °C. e) I-V curves of the cells with BCFZYN and BCFZY as air electrodes in electrolysis mode at 500 and 600 °C. f) Current densities of BCFZY, BCFZYN, and other air electrodes at 1.3 V.

Supporting Information). Under either dry or humidified oxidizing atmospheres, the BCFZYN electrode always exhibited higher k_{chem} values than that of the BCFZY electrode, confirming a higher surface exchange kinetics of the BCFZYN electrode compared to the BCFZY electrode, consistent with the above symmetric cells results.

To evaluate the potential of BCFZYN as an air electrode for PCECs, we fabricated and tested several button cells with Ni-BZCYYb, BZCYYb, and BCFZYN composite as fuel electrode, electrolyte (~19 μm) and air electrode, respectively (Fig. S8, Supporting Information). We first evaluated the cell in electrolysis mode with pure hydrogen for the fuel electrode and synthetic air (5 vol% H_2O-air) for the air electrode (Fig. S9 and Fig. S10, Supporting Information). As seen in Fig. 1e, the electrolysis current densities of the cell based BCFZYN air electrode at 1.3 V reached − 1267 and − 433 mA cm^{-2} at 600 and 500 °C, respectively, while the electrolysis current densities of the cell with the BCFZY as air electrode were only − 899 and − 277 mA cm^{-2} at 600 and 500 °C, respectively. The electrolysis performance of the cell with the BCFZYN electrode exceeded the cell with BCFZY and other reported air electrodes (Fig. 1f), confirming that the BCFZYN composite air electrode has superior OER activity [10,15,23,42,48–53]. In addition, the electrolysis current densities of the cell increased with the steam content, increasing from 10 vol % to 40 vol%, suggesting that the increase of steam concentration at the air electrode side can slightly improve the electrolysis performance of the cell (Fig. S11, Supporting Information).

3.2. Density functional theory

To gain an in-depth understanding of the ORR and OER mechanism underpinning the high performance of the BCFZYN nanocomposite, we performed DFT calculations. The 3 × 3 × 3 supercell structures of $Ba_{27}Co_{10}Fe_{10}Zr_3Y_3Ni_1O_{72}$ (pristine-BCFZYN), A-site deficient $Ba_{26}Co_{10}Fe_{10}Zr_3Y_3Ni_1O_{72}$ (D-BCFZYN), and the control sample $Ba_{27}Co_{11}Fe_{10}Zr_3Y_3O_{72}$ (BCFZY-Co11) were generated. It is worth noting that due to the existence of 27 atoms in the B-site in the 3 × 3 × 3 perovskite supercell, the control sample appears in two configurations, BCFZY-Co11 and $Ba_{27}Co_{10}Fe_{11}Zr_3Y_3O_{72}$ (BCFZY-Fe11). The experimental results confirmed that the Co-enriched BCFZY (BCFZY-Co11) had the best performance, [54] therefore, we chose BCFZY-Co11 as the control sample to further enhance the reliability of the calculation. The lowest electrostatic energy configurations were relaxed by VASP [33,34].

The oxygen vacancy formation energy, E^F_{Vo}, and hydration energy, E_{hydr}, for BCFZY-Co11, pristine-BCFZYN, and D-BCFZYN were calculated (Fig. 2a), by combining all distinct O sites in these perovskites. The calculated E^F_{Vo} values for each possible condition are shown in the Supporting Information (Fig. S12-S14, Supporting Information). For D-BCFZYN, the lowest E^F_{Vo} is 0.050 eV, which is larger than the − 0.613 eV of BCFZY-Co and the − 0.671 eV of pristine-BCFZYN. The hydration energy E_{hydr} of D-BCFZYN (−0.155 eV) is smaller than that of the other two materials (0.106 eV for pristine-BCFZYN and 0.117 eV for BCFZY-Co11). These results correlate to ASR results as Fig. 1.

The electronic density of states (DOS) is often utilized to build descriptors correlated to ORR/OER performance such as the O-*p* band

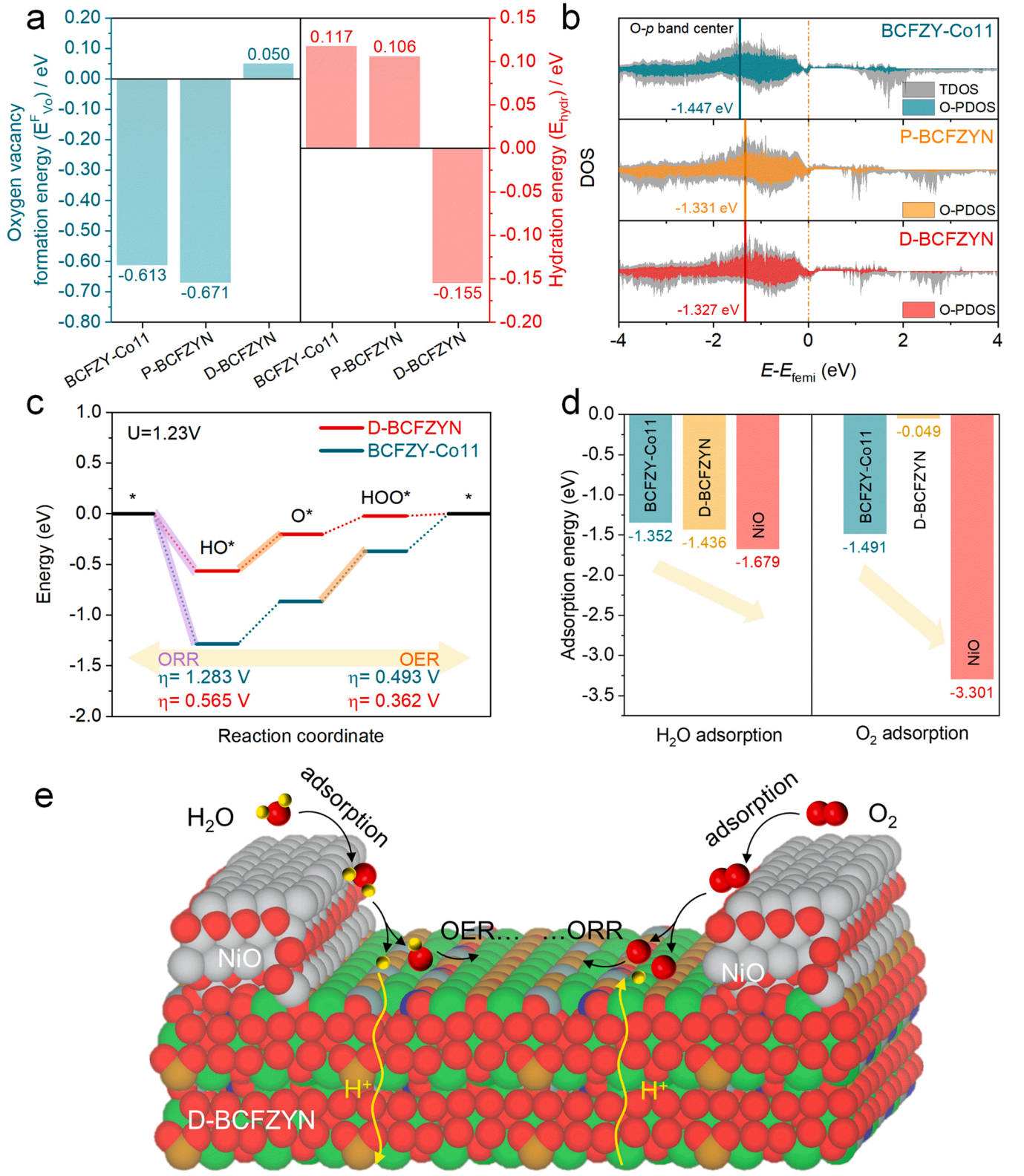

Fig. 2. a) Calculated oxygen vacancy formation energy E^F_{Vo} and hydration energy E_{hydr} for BCFZY-Co11, pristine-BCFZYN, and D-BCFZYN perovskites. b) Electronic DOS for BCFZY-Co11, pristine-BCFZYN, and D-BCFZYN perovskites. c) OER/ORR reaction pathways and free energies for BCFZY-Co11 and D-BCFZYN perovskites. d) H_2O and O_2 adsorption energies for the surface on the BCFZY-Co11, D-BCFZYN perovskites, and NiO. e) An illustration of a proposed reaction mechanism for the OER/ORR process on the surface of a nanocomposite BCFZYN air electrode.

center [55]. The O partial DOS and O-*p* band centers of BCFZY-Co11, pristine-BCFZYN, and D-BCFZYN were computed (Fig. 2b). The O-*p* band center of D-BCFZYN (−1.327 eV) is higher than pristine-BCFZYN (−1.331 eV) and BCFZY-Co11 (−1.447 eV), suggesting the higher ORR/OER activity potential of D-BCFZYN compared to BCFZY-Co11.

The ORR and OER energy barriers of D-BCFZYN and BCFZY-Co11 were also calculated, see Fig. 2c. The both overpotentials are lower for D-BCFZYN (0.362 eV OER; 0.565 eV ORR) than BCFZY-Co11 (0.493 eV OER; 1.283 eV ORR). To investigate the role of NiO on material, the steam and oxygen adsorption energies on NiO(111) were computed. Steam and oxygen adsorption energies on the NiO(111) surface were computed to be − 1.679 eV and − 3.301 eV, respectively, much smaller than those of the BCFZY-Co11 and D-BCFZYN surfaces (Fig. 2d). During OER, the NiO nanophase enhances steam adsorption, while the major D-BCFZYN perovskite phase accelerates oxygen desorption and proton conduction, enhancing OER activity; during ORR, the NiO enhances O_2 adsorption, while D-BCFZYN phase accelerates ionic (H^+/O^{2-}) conduction, enhancing ORR activity (Fig. 2e).

3.3. Phase structure and operational stability

Considering that the actual air electrode usually operates under humidified air or even high steam content air during electrolysis operation, the phase stability was investigated by the XRD data of BCFZYN exposed to 30 vol% H_2O-air for 100 h (Fig. 3a). As displayed in Fig. 3a, the phase structure of BCFZYN is unchanged, demonstrating its good phase stability. The XRD refinement data of BCFZYN before and after treatment is shown in Table S1(Supporting Information), Fig. S15 (Supporting Information) and Fig. 3b. The amount of NiO remains almost unchanged, suggesting the irreversibility of the selective exsolution, which is also a unique advantage of BCFZYN composite relative to H_2-induced exsolution [56–58].

We also evaluated the durability of the BCFZYN electrode under 30 vol% H_2O-air by impedance test of the symmetrical cell. As seen in Fig. 3c, the BCFZYN electrode exhibits a more stable long-term operational stability with an average degradation rate of 0.004 Ω cm^2 h^{-1}, which is much lower than that of the BCFZY electrode (0.019 Ω cm^2 h^{-1}), suggesting superior durability of the BCFZYN electrode. In addition, we also evaluated the operational stability of the cell with the BCFZYN air electrode exposed to 30 vol% H_2O-air in the electrolysis mode (Fig. 3d). As seen, the button cell operated stably for the test period of 372 h at electrolysis mode without degradation, further demonstrating the exceptional stability of BCFZYN air electrode in the electrolysis mode.

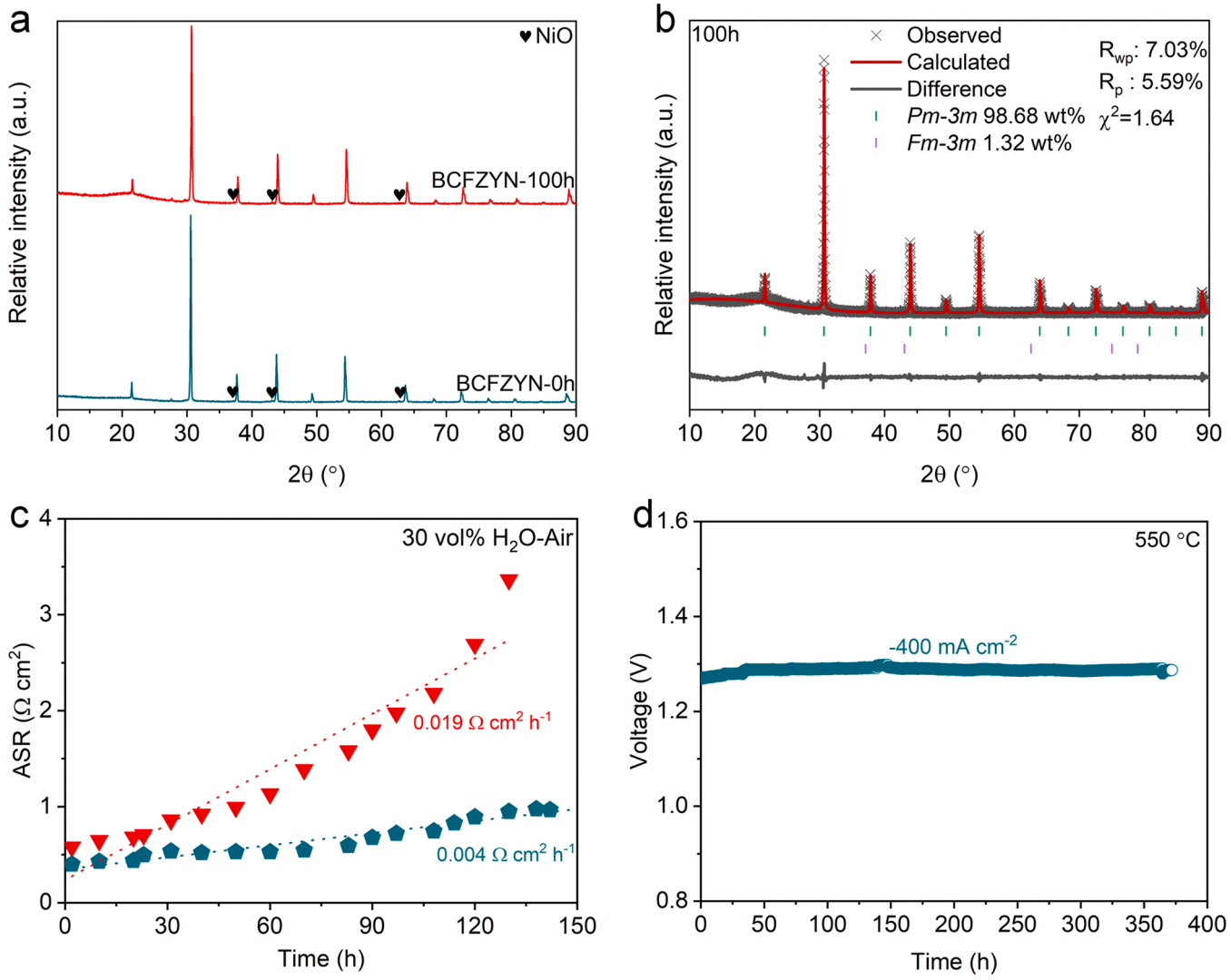

Fig. 3. a) The XRD patterns of BCFZYN before and after treatment under 30 vol% H_2O-air. b) Rietveld refinement results of BCFZYN exposed to 30 vol% H_2O-air for 100 h. c) Long-term operational stability of symmetric cells with BCFZYN and BCFZY electrodes under 30 vol% H_2O-air at 550 °C. d) Operational stability of the cell with BCFZYN as air electrode in electrolysis mode under 30 vol% H_2O-air atmospheres at 550 °C.

3.4. ORR activity and r-PCC analysis

In our previous work, we also demonstrated that the BCFZYN electrode possesses exceptional ORR activity as an air electrode of PCFCs [1]. ORR activity is also related to O_2/steam diffusion, surface exchange, and $H^+/O^{2-}/e^-$ triple conducting capability in air electrodes [46]. As mentioned above, D-BCFZYN exhibited higher oxygen desorption capability and NiO has high steam adsorption capability compared to BCFZY; it seems that these factors are beneficial to OER activity, but not conducive to ORR activity. However, under 30 vol% H_2O-air atmosphere, the decreased Rp values of the BCFZYN electrode (Fig. 1c) and decreased electrochemical resistance corresponding P2 of the BCFZYN electrode (Fig. 1d) compared to BCFZY suggests that the BCFZYN electrode exhibits a better combination of surface exchange and H^+/O^{2-} bulk diffusion capability. Furthermore, under a low steam content air atmosphere (5 vol% H_2O-air), the Rp values (Fig. S16a, Supporting Information) and the corresponding P2 (Fig. S16b, Supporting Information) of BCFZYN and BCFZY exhibit a similar pattern to that under 30 vol% H_2O-air atmospheres. The enhanced oxygen surface exchange and bulk diffusion of BCFZYN can also be confirmed by the higher k_{chem} and D_{chem} (Fig. S7, Supporting Information) values of BCZFYN under dry/-humidified atmospheres compared to that of BCFZY, while the enhanced surface exchange and proton bulk diffusion can be proved by the lower electrochemical process resistance corresponding P2 of BCFZYN under humidified N_2 compared to that of BCFZY (Fig. 1b). The better combination of surface exchange and H^+/O^{2-} bulk diffusion ability in BCFZYN were consequently also beneficial to ORR activity, resulting in the outstanding ORR activity of BCFZYN nanocomposite, as demonstrated in our previous study. Indeed, peak power densities (PPDs) of 936, 663, 427, and 252 mW cm^{-2} were achieved at 600, 550, 500, and 450 °C, respectively, for the cell operating in fuel cell mode, which is much higher than those of the similar cell with the BCFZY air electrode (Fig. 4a and Fig. S17, Supporting Information). In addition, the cell maintained a robust operational stability of 400 h (Fig. S18, Supporting Information).

Considering BCFZYN has excellent ORR/OER activities on protonic electrolytes, it may be a promising air electrode for r-PCCs. Thus, we also tested the BCFZYN in r-PCCs. Here, the I-V curves of another cell with the BCFZYN as an air electrode were obtained with hydrogen and wet air (5 vol% H_2O-air) on the air electrode. As seen in Fig. 4b, compared to the previously tested cell (Fig. S8, Supporting Information), this button cell achieved similar electrolysis performance, but a slightly lower fuel cell performance (Fig. S19, Supporting Information). The slightly decreased performance in fuel cell mode can be attributed to the introduction of steam in the air electrode, resulting in hydration, which suppressed oxygen surface exchange and bulk diffusion at a certain degree. Finally, the cell also exhibited excellent operational stability during 20 cycles (194 h) between fuel cell and electrolysis modes, further demonstrating the application potential of BCFZYN air electrode in r-PCCs technology (Fig. 4c). Table S2 (Supporting Information) lists a comparison of the performance of the most advanced air electrodes in r-PCCs as reported in the literature [10,11,14,15,23,27,42,46,47,50,51,59–63]. It demonstrates our results are among the top level performances, making BCFZYN nanocomposite a promising potential air electrode for r-PCCs with great practical application potential.

4. Conclusion

In conclusion, we have experimentally and theoretically demonstrated that the BCFZYN nanocomposite possesses excellent catalytic activity for OER at elevated temperature over protonic electrolytes, satisfying the bifunctional requirements of PCEC air electrodes. A PCEC with the BCFZYN composite as an air electrode displayed a high electrolysis current density of − 1267 mA cm^{-2} in electrolysis mode at 1.3 V at 600 °C, while maintaining exceptional durability of 372 h at 550 °C. DFT calculations suggest that the excellent OER activity is attributed to the rapid steam adsorption on the NiO nanoparticles, and fast O_2 desorption and proton conduction of D-BCFZYN major phase. In addition, an r-PCC with BCFZYN air electrode achieved exceptional durability during 194 h cycling mode between fuel cell and electrolysis modes, demonstrating the high potential of BCFZYN for use as an air electrode in r-PCCs technology.

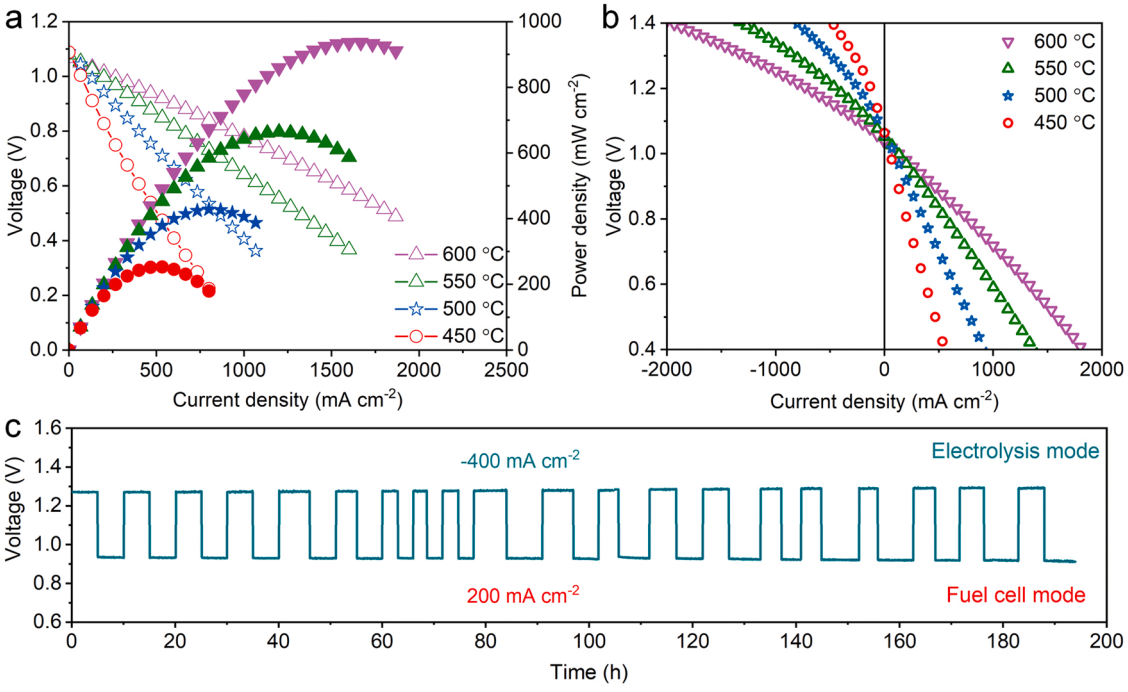

Fig. 4. a) I-V and I-P curves of Ni-BZCYYb|BZCYYb|BCFZYN button cell in fuel cell mode under H_2/dry synthetic air conditions at 450–600 °C. b) I-V curves of the second cell with BCFZYN as air electrode in reversible mode at 450–600 °C with pure hydrogen for the fuel electrode and synthetic air (5 vol% H_2O-air) for the air electrode. c) Cyclic operational stability of r-PCC with BCFZYN air electrode between fuel cell and electrolysis modes at 550 °C.

CRediT authorship contribution statement

Mingzhuang Liang: Methodology, Investigation, Data curation, Validation, Writing – original draft. **Yuhao Wang**: Software, Review. **Yufei Song**: Formal analysis, Review. **Daqin Guan**: Software. **Jie Wu**: Investigation. **Peng Chen**: Investigation. **Adeleke Maradesa**: DRT analysis. **Meigui Xu**: Resources, Funding acquisition. **Guangming Yang**: Resources. **Wei Zhou**: Data curation, Validation. **Wei Wang**: Resources. **Ran Ran**: Data curation, Validation. **Francesco Ciucci**: Review, Editing, Resources, Supervision, Funding acquisition. **Zongping Shao**: Writing – review & editing, Resources, Supervision, Funding acquisition.

Declaration of Competing Interest

The authors declare that they have no known competing financial interests or personal relationships that could have appeared to influence the work reported in this paper.

Data availability

Data will be made available on request.

Acknowledgments

M.L., Y.W., and Y.S. contributed equally to this work. The authors gratefully acknowledge the support of the National Key R&D Program of China (No. 2022YFB4002201) and the National Natural Science Foundation of China (No. 22108121, 21908106, and 21878158), Jiangsu Natural Science Foundation (No. BK20190682), and Graduate Research and Innovation Projects of Jiangsu Province (No. KYCX22_1345). This work was supported by the Research Grants Council of Hong Kong (GRF Projects: 16201820 and 16206019). This work was partly supported by the Project of Hetao Shenzhen-Hong Kong Science and Technology Innovation Cooperation Zone (HZQB-KCZYB-2020083). Y.W., Y.S., and F.C. would like to thank HKUST Fok Ying Tung Research Institute and National Supercomputing Center in Guangzhou Nansha sub-center for providing high-performance computational resources.

Appendix A. Supporting information

Supplementary data associated with this article can be found in the online version at doi:10.1016/j.apcatb.2023.122682.

References

[1] M. Liang, Y. Zhu, Y. Song, D. Guan, Z. Luo, G. Yang, S.P. Jiang, W. Zhou, R. Ran, Z. Shao, A new durable surface nanoparticles-modified perovskite cathode for protonic ceramic fuel cells from selective cation exsolution under oxidizing atmosphere, Adv. Mater. 34 (2021) 2106379, https://doi.org/10.1002/adma.202106379.

[2] S.H. Jensen, C. Graves, M. Mogensen, C. Wendel, R. Braun, G. Hughes, Z. Gao, S. A. Barnett, Large-scale electricity storage utilizing reversible solid oxide cells combined with underground storage of CO_2 and CH4, Energy Environ. Sci. 8 (2015) 2471–2479, https://doi.org/10.1039/C5EE01485A.

[3] C. Duan, R. Kee, H. Zhu, N. Sullivan, L. Zhu, L. Bian, D. Jennings, R. O'Hayre, Highly efficient reversible protonic ceramic electrochemical cells for power generation and fuel production, Nat. Energy 4 (2019) 230–240, https://doi.org/10.1038/s41560-019-0333-2.

[4] M.A. Laguna-Bercero, H. Monzón, A. Larrea, V.M. Orera, Improved stability of reversible solid oxide cells with a nickelate-based oxygen electrode, J. Mater. Chem. A 4 (2016) 1446–1453, https://doi.org/10.1039/C5TA08531D.

[5] Z. Chen, L. Jiang, S. He, C. Guan, Y. Zou, Z. Yue, N. Ai, S.P. Jiang, Y. Shao, K. Chen, Development of intertwined nanostructured multi-phase air electrodes for efficient and durable reversible solid oxide cells, Appl. Catal. B 305 (2022), 121056, https://doi.org/10.1016/j.apcatb.2021.121056.

[6] J. Cao, Y. Ji, Z. Shao, Perovskites for protonic ceramic fuel cells: a review, Energy Environ. Sci. 15 (2022) 2200–2232, https://doi.org/10.1039/D2EE00132B.

[7] I. Zvonareva, X.Z. Fu, D. Medvedev, Z. Shao, Electrochemistry and energy conversion features of protonic ceramic cells with mixed ionic-electronic electrolytes, Energy Environ. Sci. 15 (2022) 439–465, https://doi.org/10.1039/D1EE03109K.

[8] W. Zhang, Y. Zhou, E. Liu, Y. Ding, Z. Luo, T. Li, N. Kane, B. Zhao, Y. Niu, Y. Liu, M. Liu, A highly efficient and durable air electrode for intermediate-temperature reversible solid oxide cells, Appl. Catal. B 299 (2021), 120631, https://doi.org/10.1016/j.apcatb.2021.120631.

[9] R. Murphy, Y. Zhou, L. Zhang, L. Soule, W. Zhang, Y. Chen, M. Liu, A new family of proton-conducting electrolytes for reversible solid oxide cells: BaHfxCe0.8-xY0.1Yb0.1O3-δ, Adv. Funct. Mater. 30 (2020) 2002265, https://doi.org/10.1002/adfm.202002265.

[10] Z. Liu, D. Cheng, Y. Zhu, M. Liang, M. Yang, G. Yang, R. Ran, W. Wang, W. Zhou, Z. Shao, Robust bifunctional phosphorus-doped perovskite oxygen electrode for reversible proton ceramic electrochemical cells, Chem. Eng. J. 450 (2022), 137787, https://doi.org/10.1016/j.cej.2022.137787.

[11] K. Pei, Y. Zhou, K. Xu, H. Zhang, Y. Ding, B. Zhao, W. Yuan, K. Sasaki, Y. Choi, Y. Chen, M. Liu, Surface restructuring of a perovskite-type air electrode for reversible protonic ceramic electrochemical cells, Nat. Commun. 13 (2022) 1–10, https://doi.org/10.1038/s41467-022-29866-5.

[12] D. Kim, K.T. Bae, K.J. Kim, H. Im, S. Jang, S. Oh, S.W. Lee, T.H. Shin, K.T. Lee, High-performance protonic ceramic electrochemical cells, ACS Energy Lett 7 (2022) 2393, https://doi.org/10.1021/acsenergylett.2c01370.

[13] M. Liang, Y. Song, D. Liu, L. Xu, M. Xu, G. Yang, W. Wang, W. Zhou, R. Ran, Z. Shao, Magnesium tuned triple conductivity and bifunctionality of BaCo0.4Fe0.4Zr0.1Y0.1O3-δ perovskite towards reversible protonic ceramic electrochemical cells, Appl. Catal. B 318 (2022), 121868, https://doi.org/10.1016/j.apcatb.2022.121868.

[14] Y. Niu, Y. Zhou, W. Zhang, Y. Zhang, C. Evans, Z. Luo, N. Kane, Y. Ding, Y. Chen, X. Guo, W. Lv, M. Liu, Highly active and durable air electrodes for reversible protonic ceramic electrochemical cells enabled by an efficient bifunctional catalyst, Adv. Energy Mater. 12 (2022) 2103783, https://doi.org/10.1002/aenm.202103783.

[15] H. Ding, W. Wu, C. Jiang, Y. Ding, W. Bian, B. Hu, P. Singh, C.J. Orme, L. Wang, Y. Zhang, D. Ding, Self-sustainable protonic ceramic electrochemical cells using a triple conducting electrode for hydrogen and power production, Nat. Commun. 11 (2020) 1–11, https://doi.org/1038/s41467-020-15677-z.

[16] a) W. Zhan, Y. Zhou, T. Chen, G. Miao, X. Ye, J. Li, Z. Zhan, S. Wang, Z. Deng, Long-term stability of infiltrated La0.8Sr0.2CoO3-δ, La0.58Sr0.4Co0.2Fe0.8O3-δ and SmBa0.5Sr0.5Co2.0O5+δ cathodes for low temperature solid oxide fuel cells, Int. J. Hydrog. Energy 40 (2015) 16532–16539, https://doi.org/10.1016/j.ijhydene.2015.08.073;
b) V.I. Sharma, B. Yildiz, Degradation mechanism in La0.8Sr0.2CoO3 as contact layer on the solid oxide electrolysis cell anode, J. Electrochem. Soc. 157 (2010) B441, https://doi.org/10.1149/1.3288835.

[17] a) M. Liu, D. Ding, K. Blinn, X. Li, L. Nie, M. Liu, Enhanced performance of LSCF cathode through surface modification, Int. J. Hydrog. Energy 37 (2012) 8613–8620, https://doi.org/10.1016/j.ijhydene.2012.02.139;
b) S.J. Kim, G.M. Choi, Stability of LSCF electrode with GDC interlayer in YSZ-based solid oxide electrolysis cell, Solid State Ion. 262 (2014) 303–306, https://doi.org/10.1016/j.ssi.2014.01.001.

[18] a) Z. Shao, M.H. Sossina, A high-performance cathode for the next generation of solid-oxide fuel cells, Nature 431 (2004) 170–173, https://doi.org/10.1038/nature02863;
b) P. Kim-Lohsoontorn, D.J.L. Brett, N. Laosiripojana, Y.-M. Kim, J.-M. Bae, Performance of solid oxide electrolysis cells based on composite La0.8Sr0.2MnO3-δ - yttria stabilized zirconia and Ba0.5Sr0.5Co0.8Fe0.2O3-δ oxygen electrodes, Int. J. Hydrog. Energy 35 (2010) 3958–3966, https://doi.org/10.1016/j.ijhydene.2010.02.039.

[19] Z. Hui, P. Michèle, Preparation, chemical stability, and electrical properties of Ba(Ce1-xBix)O3 (x= 0.0-0.5), J. Mater. Chem. 12 (2002) 3787–3791, https://doi.org/10.1039/B205107A.

[20] Y. Rao, S. Zhong, F. He, Z. Wang, R. Peng, Y. Lu, Cobalt-doped BaZrO3: a single phase air electrode material for reversible solid oxide cells, Int. J. Hydrog. Energy 37 (2012) 12522–12527, https://doi.org/10.1016/j.ijhydene.2012.05.022.

[21] E. Fabbri, I. Markus, L. Bi, D. Pergolesi, E. Traversa, Exploring mixed protonic/electronic conducting oxides as cathode materials for intermediate temperature SOFCs based on proton conducting electrolytes, ECS Trans. 35 (2011) 2305, https://doi.org/10.1149/1.3570226.

[22] L. Yang, S. Wang, X. Lou, M. Liu, Electrical conductivity and electrochemical performance of cobalt-doped BaZr0.1Ce0.7Y0.2O3-δ cathode, Int. J. Hydrog. Energy 36 (2011) 2266–2270, https://doi.org/10.1016/j.ijhydene.2010.11.053.

[23] a) H. Kim, S. Joo, O. Kwon, S. Choi, G. Kim, Cobalt-free Pr0.5Ba0.4Sr0.1FeO3-δ as a highly efficient cathode for commercial YSZ-supported solid oxide fuel cell, ChemElectroChem 7 (2020) 4378–4382, https://doi.org/10.1002/celc.202001240;
b) J. Kim, A. Junb, O. Gwon, S. Yoo, M. Liu, J. Shin, T.-H. Lim, G. Kim, Hybrid-solid oxide electrolysis cell: a new strategy for efficient hydrogen production, Nano Energy 44 (2018) 121–126, https://doi.org/10.1016/j.nanoen.2017.11.074.

[24] a) S. Choi, C.J. Kucharczyk, Y. Liang, X. Zhang, I. Takeuchi, H.-I. Ji, S.M. Haile, Exceptional power density and stability at intermediate temperatures in protonic ceramic fuel cells, Nat. Energy 3 (2018) 202–210, https://doi.org/10.1038/s41560-017-0085-9;
b) S. Choi, T.C. Davenport, S.M. Haile, Protonic ceramic electrochemical cells for hydrogen production and electricity generation: exceptional reversibility, stability, and demonstrated faradaic efficiency, Energy Environ. Sci. 12 (2019) 206–215, https://doi.org/10.1039/C8EE02865F.

[25] Y. Song, Y. Chen, W. Wang, C. Zhou, Y. Zhong, G. Yang, W. Zhou, M. Liu, Z. Shao, Self-assembled triple-conducting nanocomposite as a superior protonic ceramic

fuel cell cathode, Joule 3 (2019) 2842, https://doi.org/10.1016/j.joule.2019.07.004.
[26] Y. Wang, K. Pei, B. Zhao, Y. Zhao, H. Wang, Q. Niu, Y. Chen, Enhanced electrochemical performance of a Ba0.5Sr0.5Co0.7Fe0.2Ni0.1O3-δ-BaZr0.1Ce0.7Y0.1Yb0.1O3-δ composite oxygen electrode for protonic ceramic electrochemical cells, Energy Fuels 35 (2021) 14101–14109, https://doi.org/10.1021/acs.energyfuels.1c02148.
[27] Y. Zhou, W. Zhang, N. Kane, Z. Luo, K. Pei, K. Sasaki, Y. Choi, Y. Chen, D. Ding, M. Liu, An efficient bifunctional air electrode for reversible protonic ceramic electrochemical cells, Adv. Funct. Mater. 31 (2021) 2105386, https://doi.org/10.1002/adfm.202105386.
[28] S. Yang, S. Zhang, C. Sun, X. Ye, Z. Wen, Lattice incorporation of Cu2+ into the BaCe0.7Zr0.1Y0.1Yb0.1O3-δ electrolyte on boosting its sintering and proton-conducting abilities for reversible solid oxide cells, ACS Appl. Mater. Interfaces 10 (2018) 42387–42396, https://doi.org/10.1021/acsami.8b15402.
[29] R. Strandbakke, E. Vøllestad, S.A. Robinson, M.L. Fontaine, T. Norby, Ba0.5Gd0.8La0.7Co2O6-δ infiltrated in porous BaZr0.7Ce0.2Y0.1O3 backbones as electrode material for proton ceramic electrolytes, J. Electrochem. Soc. 164 (2017) F196, https://doi.org/10.1149/2.0141704jes.
[30] Q. Wang, X. Tong, S. Ricote, R. Sažinas, P.V. Hendriksen, M. Chen, Nano-LaCoO3 infiltrated BaZr0.8Y0.2O3-δ electrodes for steam splitting in protonic ceramic electrolysis cells, Adv. Powder Mater. 1 (2022), 100003, https://doi.org/10.1016/j.apmate.2021.09.003.
[31] K. Okhotnikov, T. Charpentier, S. Cadars, Supercell program: a combinatorial structure-generation approach for the local-level modeling of atomic substitutions and partial occupancies in crystals, J. Chemin. 8 (2016) 17, https://doi.org/10.1186/s13321-016-0129-3.
[32] a) G. Kresse, J. Furthmüller, Efficiency of ab-initio total energy calculations for metals and semiconductors using a plane-wave basis set, Comput. Mater. Sci. 6 (1996) 15–50, https://doi.org/10.1016/0927-0256(96)00008-0;
b) G. Kresse, J. Hafner, Ab initio molecular dynamics for open-shell transition metals, Phys. Rev. B 48 (1993) 13115–13118, https://doi.org/10.1103/PhysRevB.48.13115;
c) P.E. Blöchl, Projector augmented-wave method, Phys. Rev. B 50 (1994) 17953, https://doi.org/10.1103/PhysRevB.50.17953.
[33] J.P. Perdew, K. Burke, M. Ernzerhof, Generalized gradient approximation made simple, Phys. Rev. Lett. 77 (1996) 3865, https://doi.org/10.1103/PhysRevLett.77.3865.
[34] A. Jain, S.P. Ong, G. Hautier, W. Chen, W.D. Richards, S. Dacek, S. Cholia, D. Gunter, D. Skinner, G. Ceder, Commentary: The materials project: A materials genome approach to accelerating materials innovation, APL Mater. 1 (2013), 011002, https://doi.org/10.1063/1.4812323.
[35] Z.M. Baiyee, C. Chen, F. Ciucci, A. DFT, U study of A-site and B-site substitution in BaFeO3-δ, Phys. Chem. Chem. Phys. 17 (2015) 23511–23520, https://doi.org/10.1039/C5CP02694F.
[36] A.B. Muñoz-García, M. Pavone, First-principles design of new electrodes for proton-conducting solid-oxide electrochemical cells: a-site doped Sr2Fe1.5Mo0.5O6-δ perovskite, Chem. Mater. 28 (2016) 490–500, https://doi.org/10.1021/acs.chemmater.5b03262.
[37] J.K. Nørskov, J. Rossmeisl, A. Logadottir, L. Lindqvist, J.R. Kitchin, T. Bligaard, H. Jónsson, Origin of the overpotential for oxygen reduction at a fuel-cell cathode, J. Phys. Chem. B 108 (2004) 17886–17892, https://doi.org/10.1021/jp047349j.
[38] J. Rossmeisl, A. Logadottir, J.K. Nørskov, Electrolysis of water on (oxidized) metal surfaces, Chem. Phys. 319 (2005) 178–184, https://doi.org/10.1016/j.chemphys.2005.05.038.
[39] S.H. Kim, K.B. Shim, C.S. Kim, J. Chou, T. Oshima, Y. Shiratori, K. Ito, K. Sasaki, Degradation of solid oxide fuel cell cathodes accelerated at a high water vapor concentration, J. Fuel Cell Sci. Technol. 7 (2010), 021011, https://doi.org/10.1115/1.3117608.
[40] R. Liu, S.H. Kim, S. Taniguchi, T. Oshima, Y. Shiratori, K. Ito, K. Sasaki, Influence of water vapor on long-term performance and accelerated degradation of solid oxide fuel cell cathodes, J. Power Sources 196 (2011) 7090–7096, https://doi.org/10.1016/j.jpowsour.2010.08.014.
[41] M. Liang, D. Liu, Y. Zhu, W. Zhou, G. Yang, R. Ran, Z. Shao, Nickel doping manipulation towards developing high-performance cathode for proton ceramic fuel cells, J. Electrochem. Soc. 169 (2022), 094509, https://doi.org/10.1149/1945-7111/ac9088.
[42] J. Shin, H. Park, K. Park, M. Saqib, M. Jo, J.H. Kim, H.-T. Lim, M. Kim, J.-Y. Kim, J. Park, Activity of layered swedenborgite structured Y0.8Er0.2BaCo3.2Ga0.8O7+δ for oxygen electrode reactions in at intermediate temperature reversible ceramic cells, J. Mater. Chem. A 9 (2021) 607–621, https://doi.org/10.1039/D0TA11000K.
[43] E. Quattrocchi, T.H. Wan, A. Belotti, D. Kim, S. Pepe, S.V. Kalinin, M. Ahmadi, F. Ciucci, The deep-DRT: a deep neural network approach to deconvolve the distribution of relaxation times from multidimensional electrochemical impedance spectroscopy data, Electrochim. Acta 392 (2021), 139010, https://doi.org/10.1016/j.electacta.2021.139010.
[44] M. Saccoccio, T.H. Wan, C. Chen, F. Ciucci, Optimal regularization in distribution of relaxation times applied to electrochemical impedance spectroscopy: ridge and lasso regression methods-a theoretical and experimental study, Electrochim. Acta 147 (2014) 470–482, https://doi.org/10.1016/j.electacta.2014.09.058.
[45] T. Wan, M. Saccoccio, C. Chen, F. Ciucci, Influence of the discretization methods on the distribution of relaxation times deconvolution: implementing radial basis functions with DRTtools, Electrochim. Acta 184 (2015) 483–499, https://doi.org/10.1016/j.electacta.2015.09.097.
[46] R. Ren, Z. Wang, C. Xu, W. Sun, J. Qiao, D.W. Rooney, K. Su, Tuning the defects of the triple conducting oxide BaCo0.4Fe0.4Zr0.1Y0.1O3-δ perovskite toward enhanced cathode activity of protonic ceramic fuel cells, J. Mater. Chem. A 7 (2019) 18365–18372, https://doi.org/10.1039/c9ta04335g.
[47] H. Tong, M. Fu, Y. Yang, F. Chen, Z. Tao, A novel self-assembled cobalt-free perovskite composite cathode with triple-conduction for intermediate proton-conducting solid oxide fuel cells, Adv. Funct. Mater. 24 (2022) 2209695, https://doi.org/10.1002/adfm.202209695.
[48] Z. Liu, Y. Chen, G. Yang, M. Yang, R. Ji, Y. Song, R. Ran, W. Zhou, Z. Shao, One-pot derived thermodynamically quasi-stable triple conducting nanocomposite as robust bifunctional air electrode for reversible protonic ceramic cells, Appl. Catal. B 319 (2022), 121929, https://doi.org/10.1016/j.apcatb.2022.121929.
[49] W. Tang, H. Ding, W. Bian, W. Wu, W. Li, X. Liu, J.Y. Gomez, C.Y.R. Vera, M. Zhou, D. Ding, Understanding of A-site deficiency in layered perovskites: promotion of dual reaction kinetics for water oxidation and oxygen reduction in protonic ceramic electrochemical cells, J. Mater. Chem. A 8 (2020) 14600–14608, https://doi.org/10.1039/D0TA05137C.
[50] Y. Meng, J. Gao, H. Huang, M. Zou, J. Duffy, J. Tong, K.S. Brinkman, A high-performance reversible protonic ceramic electrochemical cell based on a novel Sm-doped BaCe0.7Zr0.1Y0.2O3-δ electrolyte, J. Power Sources 439 (2019), 227093, https://doi.org/10.1016/j.jpowsour.2019.227093.
[51] L. Lei, Z. Tao, X. Wang, J.P. Lemmon, F. Chen, Intermediate-temperature solid oxide electrolysis cells with thin proton-conducting electrolyte and a robust air electrode, J. Mater. Chem. A 5 (2017) 22945–22951, https://doi.org/10.1039/C7TA05841A.
[52] D. Huan, W. Wang, Y. Xie, N. Shi, Y. Wan, C. Xia, R. Peng, Y. Lu, Investigation of real polarization resistance for electrode performance in proton-conducting electrolysis cells, J. Mater. Chem. A 6 (2018) 18508–18517, https://doi.org/10.1039/C8TA06862C.
[53] Y. Song, J. Liu, Y. Wang, D. Guan, A. Seong, M. Liang, M. Robson, X. Xiong, Z. Zhang, G. Kim, Z. Shao, F. Ciucci, Nanocomposites: a new opportunity for developing highly active and durable bifunctional air electrodes for reversible protonic ceramic cells, Adv. Energy Mater. 11 (2021) 2101899, https://doi.org/10.1002/aenm.202101899.
[54] M.C. Papac, K.R. Talley, R. O'Hayre, A. Zakutayev, Instrument for spatially resolved, temperature-dependent electrochemical impedance spectroscopy of thin films under locally controlled atmosphere, Rev. Sci. Instrum. 92 (2021), 065105, https://doi.org/10.1063/5.0024875.
[55] a) R. Jacobs, J. Hwang, Y. Shao-Horn, D. Morgan, Assessing correlations of perovskite catalytic performance with electronic structure descriptors, Chem. Mater. 31 (2019) 785–797, https://doi.org/10.1021/acs.chemmater.8b03840;
b) Y. Lee, J. Kleis, J. Rossmeisl, Y. Shao-Horn, D. Morgan, Prediction of solid oxide fuel cell cathode activity with first-principles descriptors, Energy Environ. Sci. 4 (2011) 3966–3970, https://doi.org/10.1039/C1EE02032C.
[56] K. Lai, A. Manthiram, Evolution of exsolved nanoparticles on a perovskite oxide surface during a redox process, Chem. Mater. 30 (2018) 2838–2847, https://doi.org/10.1021/acs.chemmater.8b01029.
[57] H. Lv, T. Liu, X. Zhang, Y. Song, H. Matsumoto, N. Ta, C. Zeng, G. Wang, X. Bao, Atomic-scale insight into exsolution of CoFe alloy nanoparticles in La0.4Sr0.6Co0.2Fe0.7Mo0.1O3-δ with efficient CO_2 electrolysis, Angew. Chem. Int. Ed. 59 (2020) 15968–15973, https://doi.org/10.1002/anie.202006536.
[58] H. Lv, L. Lin, X. Zhang, Y. Song, H. Matsumoto, C. Zeng, N. Ta, W. Liu, D. Gao, G. Wang, X. Bao, In situ investigation of reversible exsolution/dissolution of CoFe alloy nanoparticles in a Co-doped Sr2Fe1.5Mo0.5O6-δ cathode for CO_2 electrolysis, Adv. Mater. 32 (2020) 1906193, https://doi.org/10.1002/adma.201906193.
[59] K. Xu, H. Zhang, Y. Xu, F. He, Y. Zhou, Y. Pan, J. Ma, B. Zhao, W. Yuan, Y. Chen, M. Liu, An efficient steam-induced heterostructured air electrode for protonic ceramic electrochemical cells, Adv. Funct. Mater. (2022) 2110998, https://doi.org/10.1002/adfm.202110998.
[60] J. Lee, K. Park, H. Park, H. Bae, M. Saqib, K. Park, J. Shin, M. Jo, J. Kim, S. Song, E. D. Wachsman, J. Park, Triple perovskite structured Nd1.5Ba1.5CoFeMnO9-δ oxygen electrode materials for highly efficient and stable reversible protonic ceramic cells, J. Power Sources 510 (2021), 230409, https://doi.org/10.1016/j.jpowsour.2021.230409.
[61] F. He, S. Liu, T. Wu, M. Yang, W. Li, G. Yang, F. Zhu, H. Zhang, K. Pei, Y. Chen, W. Zhou, Z. Shao, Catalytic self-assembled air electrode for highly active and durable reversible protonic ceramic electrochemical cells, Adv. Funct. Mater. (2022) 2206756, https://doi.org/10.1002/adfm.202206756.
[62] Y. Zhou, E. Liu, Y. Chen, Y. Liu, L. Zhang, W. Zhang, Z. Luo, N. Kane, B. Zhao, L. Soule, Y. Niu, Y. Ding, H. Ding, D. Ding, M. Liu, An active and robust air electrode for reversible protonic ceramic electrochemical cells, ACS Energy Lett. 6 (2021) 1511–1520, https://doi.org/10.1021/acsenergylett.1c00432.
[63] N. Wang, H. Toriumi, Y. Sato, C. Tang, T. Nakamura, K. Amezawa, S. Kitano, H. Habazaki, Y. Aoki, La0.8Sr0.2Co1-xNixO3-δ as the efficient triple conductor air electrode for protonic ceramic cells, ACS Appl. Energy Mater. 4 (2021) 554–563, https://doi.org/10.1021/acsaem.0c02447.